A 'one-two punch' therapy strategy to target chemoresistance in ER+ breast cancer

Feng Chi[1], Jiayi Liu[2], Samuel W. Brady[3], Patrick A. Cosgrove[1], Aritro Nath[1], Jasmine A. McQuerry[1, 3 4], Sumana Majumdar[1], Philip J. Moos[4], Jeffrey T. Chang[2], Michael Kahn[5], Andrea H.Bild[1*]

[1] Department of Medical Oncology & Therapeutics Research, City of Hope National Medical Center, 1500 East Duarte Road, Duarte, CA 91010, USA.

[2] Department of Integrative Biology and Pharmacology, School of Medicine, School of Biomedical Informatics, UT Health Sciences Center at Houston, Houston, TX 77030, USA.

3 Department of Oncological Sciences, School of Medicine, University of Utah, 2000 Circle of Hope Drive, Salt Lake City, UT 84112, USA.

[4] Department of Pharmacology and Toxicology, College of Pharmacy, University of Utah, 30 South 2000 East, Salt Lake City, UT 84112, USA.

[5] Department of Molecular Medicine, City of Hope National Medical Center, 1500 East Duarte Road, Duarte, CA 91010, USA.

***Corresponding Authors**: Andrea Bild, Ph.D.
Professor
Department of Medical Oncology and Therapeutics
City of Hope Comprehensive Cancer Institute
1218 S Fifth Ave, Monrovia, CA 91016
Email: abild@coh.org

Short Title: A 'one-two punch' therapy strategy to halt resistance

Abstract

Cancer cell phenotypes evolve during a tumor's treatment. In some cases, tumor cells acquire cancer stem cell-like (CSL) traits such as resistance to chemotherapy and diminished differentiation; therefore, targeting these cells may be therapeutically beneficial. In this study, we show that in progressive estrogen receptor positive (ER+) metastatic breast cancer patients, resistant tumor subclones that emerge following chemotherapy have increased CSL abundance. Further, in vitro organoid growth of ER+ patient cancer cells also shows that chemotherapy treatment leads to increased abundance of ALDH+/CD44+ CSL cells. Chemotherapy induced CSL abundance is blocked by treatment with an HDAC inhibitor, belinostat. Further, belinostat treatment diminished both mammosphere formation and size following chemotherapy, also indicating a decrease in progenitor CSL traits. Single-cell RNA sequencing analysis with patient samples showed that HDAC targets and MYC signaling were promoted by chemotherapy and inhibited upon belinostat treatment. These findings indicate that HDAC inhibition can block chemotherapy-induced drug resistant phenotypes with 'one-two punch' strategy in refractory breast cancer cells.

Keywords: CSL, ALDH, CD44, chemotherapy, single-cell RNA-seq, HDAC, belinostat, MYC, chemoresistance

46 **Introdution**

47 Breast cancer is the most frequently diagnosed and second leading cause of cancer-related deaths
48 in women (1). Chemotherapy kills cancer cells by inducing apoptosis through DNA damage and/or
49 mitotic division inhibition (2). Chemotherapeutics are often standard of care in clinical oncology because
50 of their effectiveness in reducing tumor burden and improving survival (3). Nevertheless, some patients
51 will recur with metastatic progression, which has a 90% of cancer mortality (4), resulting in a 23% 5-year
52 survival rate for these breast cancer patients (1).

53 Tumors are composed of heterogeneous populations of cells, thought to have a hierarchical
54 organization driven by cancer stem cells (CSCs). CSCs are a small therapy-resistant sub-population of
55 cells within tumors that possess the capacity of self-renewal and are capable of promoting a refractory
56 state in patients following drug treatment (5). These CSCs can initiate a new primary tumor, bear an
57 inherent resistance to chemotherapeutic drugs, and contribute to recurrent disease (6). Breast CSCs
58 (BCSCs) exhibit a CD44 high/CD24 low phenotype with high ALDH1 expression (ALDH1+) (7). Tumor
59 cells can also acquire stem cell like characteristics, such as expression of progenitor markers and drug
60 resistance. These cells may represent a de-differentiated state similar to CSCs and reflect a more primitive
61 tumor cell progenitor (8).

62 Based on the mechanisms of action, chemotherapies could be divided into at least three major
63 groups: antimetabolites; genotoxic agents (eg. doxorubicin serving as alkylating agent, which inhibits
64 DNA topoisomerase II and induces DNA damage and apoptosis; carboplatin serving as intercalating
65 agent, which binds in the grooves in the DNA helix and interfering with polymerase activity during
66 replication/transcription); and mitotic spindle inhibitors (eg. paclitaxel, which disrupts mitosis by
67 affecting the formation/function of spindle microtubule fibers required for chromosome alignment) (9).
68 Some resistance mechanisms have been described for these chemotherapies. For example,
69 chemoresistance can be acquired by altered membrane transport through ABCB1 (P-gp or MDR1) for
70 doxorubicin and paclitaxel (9), and enhanced DNA repair through increased level of excision repair cross-

complementing protein (ERCC1) for carboplatin (10). Current chemotherapeutic regimens target the bulk of the tumor cells and may benefit from also targeting resistant cells, such as cancer stem cells (CSC) or cancer cells that have stem-like traits such as drug resistance or de-differentiated states (11). Failure to eliminate these cells can lead to drug resistance, subsequent recurrence and metastasis (12), suggesting that targeting these populations may be necessary to improve outcomes (5, 13). Multiple strategies have been proposed to combat CSCs; however, clinical implementation has remained elusive (7, 14). A strategy combining conventional cytotoxic chemotherapy and anti-CSC compounds could increase efficacy in reducing the risk of breast cancer relapse and metastasis (7). The drug-tolerant phenotype within a small subpopulation of cancer cells have been found transiently acquired and reversible, which could be selectively ablated by chromatin-modifying agents, such as HDAC inhibitor, suggesting a potential therapeutic opportunity with 'one-two punch' strategy (15).

Single-cell sequencing techniques have been leveraged to identify resistant cancer evolution upon chemotherapy treatment (16-19). Previously, we performed whole-genome sequencing (WGS) and single-cell RNA-Seq (scRNA-Seq) on four patients' matched pre-treatment (chemo-sensitive) and post-treatment (chemo-resistant) samples to investigate the mechanisms of acquired chemotherapy resistance in breast cancer. Three of four patients demonstrated increased post-treatment stem cell-like and mesenchymal properties, which may have promoted acquired drug resistance in these patients (19). Based on this data, we sought to understand how multiple different chemotherapies impact CSL state and determine therapy approaches to prevent emergence of CSL cells. Here, we find that chemotherapies with different mechanisms of action can select for subclones with primitive traits through transcriptional changes. Belinostat, an HDAC inhibitor, was found to prevent this selection and reverse CSL therapy resistance signaling, such as signaling in MYC and dedifferentiation pathways.

In total, this research provides the following unique findings: 1) a novel one-two, chemo-belinostat combination therapy strategy to target chemo-treatment acquired stemness, 2) the ability of belinostat to serve as a common anti-CSL inhibitor following multiple chemotherapies, 3) the specificity

97 of HDAC inhibitors to target the stemness phenotypic shift and not just a change in tumor cell viability
98 and/or apoptosis, 4) the use of patient tumor samples to validate that stemness enrichment in subclonal
99 populations of patients is linked to their survival during chemotherapy, and 5) an understanding of the
100 transcriptional changes in single tumor cells upon CSL phenotype reversal. Taken together, these findings
101 could help to build a new strategy consisting of sequential chemotherapy and HDAC inhibitor
102 combination treatment to combat refractory breast cancer.
103
104
105 **Results**

106 **Resistant subclones are enriched in CSL cells**

107 To test how chemotherapy selects for resistant cell traits, we studied CSL characteristics in tumor
108 subclones prior to treatment using four breast cancer patients using copy-number variations (CNV) from
109 WGS (19). Importantly, while challenging, these studies leverage actual patient tumor phenotype and
110 subclonal evolution during long courses of treatment, for which in vitro work is no substitute. The
111 treatment history for these four ER+ patients and the time points at which analysis was performed are
112 shown in Fig. S1A. To obtain CSL and non-CSL populations, tumor cells collected from each patient
113 were sorted for ALDH and CD44 expression, and cells were isolated to four quadrants (ALDH+/CD44+
114 CSL cells, ALDH+/CD44- cells, ALDH-/CD44+ cells, and ALDH-/CD44- cells) (Fig. S1B). We defined
115 the CSL population as ALDH+/CD44+ cells (20). DNA from cells belonging to each of these quadrants
116 was isolated and subjected to low-coverage WGS (2X to 10X) in order to infer copy number variants
117 (CNVs) and determine the prevalence of each subclonal CNV in each cancer stem population (see Fig.
118 S1C). The evolution of subclones is shown in Fig. S1D, E, F, G and described in the Methods. We
119 identified subclone-specific CNVs in each patient at each time point, and then assessed each subclone for
120 the presence of CSL vs. non-CSL populations to determine whether subclones that survive chemotherapy
121 and are also present at time of recurrence had increased numbers of CSL cells. In two of four patients that

122 are progressing on chemotherapy (Patient#1 and Patient#2), the tumor subclone that survives treatment
123 and becomes resistant to chemotherapy has increased CSL abundance compared to other non-resistant
124 subclones (Fig. 1A), suggesting genetic selection can enrich CSL cells in post-treatment resistant
125 subclones in ER+ breast cancer. This result supports our published research showing that patients treated
126 over years of treatments show enrichment in stemness phenotypes (19).

127

128 **Chemotherapy-induced feedback increases CSL traits in patient tumor cells**

129 Our previous research demonstrates increased post-treatment stem cell-like properties in three of
130 four patients, including the Patient#1 and Patient#2 used in this work (19). These findings indicate that
131 the increase in post-treatment CSL cell abundance may be due to chemotherapy-induced feedback. To test
132 this hypothesis, we again use patient cancer cells obtain from malignant pleural effusions or ascites, as
133 these samples may best reflect physiologically relevant phenotypes and signaling changes during drug
134 treatment. These samples were treated with three different chemotherapies of various mechanisms of
135 action (doxorubicin, carboplatin, and paclitaxel) for 72 hours, followed by flow cytometry to measure the
136 CSL abundance using the FACS gating strategy shown in Fig. S2A. Five ER+, PR+, Her2- and three
137 TNBC (triple-negative breast cancer) patient tumor samples were used to test if chemotherapy could
138 induce CSL cells. Doxorubicin, carboplatin, and paclitaxel were used to treat the patient cultures in 3D
139 organoids at indicated doses. In the five ER+ patient cultures (Patient##5, Patient#6, Patient#7, Patient#8,
140 and Patient#9), all three chemotherapies increased the proportion of ALDH+/CD44+ CSL cells versus
141 live cells (CSL cells/Live) (Fig. 1B). This was confirmed with ALDH+/CD44+ CSL cells versus total
142 cells (CSL cells/Total) (Fig. S2B), although the CSL cells versus live cells and versus total cells were
143 reduced by carboplatin in Patient#6. Interestingly, for three TNBC patient samples, the mean values of
144 ALDH, the ALDH+/CD44+ CSL cells versus live cells and total cells were generally decreased. These
145 results suggest that there is heterogeneity in how chemotherapy impacts CSL state. Further, the results
146 from patient tumor cells show that chemotherapy induces CSL traits in ER+ breast cancer.

147

148 **Chemotherapy-induced CSL states are recapitulated in breast cancer cell lines**

149 To further investigate these phenomena, we tested four ER+ breast cancer cell lines (CAMA-1,
150 T47D, MCF-7, ZR-75-1) and five TNBC cell lines (MDA-MB-231, BT549, HCC38, HCC1395,
151 HCC1143) using the same experimental settings. As shown in Fig. 1C and Fig. S2C, chemotherapy
152 increased the abundance of ALDH, CD44, CSL cells/Live, and CSL cells/Total in most ER+ cell lines,
153 although T47D and MCF7 have been reported as ALDH-negative (21). This promotion was less present
154 in TNBC cell lines following chemotherapy, and showed only increased abundance of CD44. The CSL
155 enrichment by chemotherapy in ER+ cells and TNBC is shown by relative mean values of ALDH and
156 CD44, which are highlighted for ER+ patient cells (Fig. S3A), TNBC patient cells (Fig. S3B), ER+ cell
157 lines (Fig. S3C), and TNBC cell lines (Fig. S3D). Spots for TNBC patients and cell lines showed a lesser
158 extent of primitive cell traits compared to ER+ cells. These studies indicate that chemotherapy can lead to
159 enrichment in CSL cells and ER+ cells in particular.

160

161 **CSL phenotypes are reversed with an HDAC inhibitor**

162 We sought to find an inhibitor that could reverse chemotherapy induced CSL cells. We used an
163 ER+ breast cancer cell line CAMA-1 (ER+, PR+, and HER2-) and TNBC cell line MDA-MB-231 to test
164 for CSL reversal using a 3D organoid culture model for the chemotherapy induced CSL state. The
165 potential CSL inhibitors were selected based multiple lines of data: 1) potential strategies to suppress
166 CSCs summarized by Lin et al.,(14) and others, which include targeting pathways that regulate EMT such
167 as hedgehog (vismodegib), Wnt/β-catenin (ICG-001) or CSC markers (disulfiram as an ALDH inhibitor),
168 2) targeting histone deacetylases which may modulate stem-like signaling pathways (belinostat and
169 entinostat), 3) growth factor receptor pathway inhibitors such as AXL inhibitors (BGB324 and TP-0903),
170 FGFR inhibitor (AZD4547), EGFR inhibitors (afatinib and gefitinib), and 4) cyclin-dependent kinases
171 (CDKs) inhibitors (senexin A, ribociclib and abemaciclib), which are reported to play indispensable roles
172 in processes of stem cell self-renewal (22).

173 For CSL inhibitor selection, 3D organoids of CAMA-1 (ER+) cells and MDA-MB-231 (TNBC)
174 cells were treated with chemotherapy for 72 hours, followed by belinostat for another 72 hours, and
175 subjected to ALDEFLUOR/CD44/DAPI staining for FACS analysis. As shown in Fig. 2A, B, the HDAC
176 inhibitor belinostat consistently reversed both ALDH and CD44 levels promoted by three chemotherapy
177 treatments in both cell lines. The AXL inhibitor TP-0903 showed some reversal potential only in ER+
178 breast cancer cells. Additionally, an increased cytotoxicity of belinostat and TP-0903 were also observed
179 in the viability heat maps for both cell lines at the doses for CSL reversal effect (Fig. 2A, B). Taken
180 together, these data indicate that belinostat may serve as a general anti-chemo-induced CSL modifier in
181 breast cancer. To further evaluate the potential of belinostat to enact chemo-induced CSL reversal, we
182 performed a time-course FACS analysis from Day 1 to Day 6 to measure the CSL phenotype every day
183 using the experiment strategy shown in Fig. 3A. For the ER+ breast cancer cell line CAMA-1, as shown
184 in Fig. S4A, FACS analysis showed steadily increasing ALDH levels with all three chemotherapies
185 (doxorubicin, carboplatin, and paclitaxel) from D 1 to Day 6, while the CD44 levels showed a more
186 pulse-like pattern with increased levels from Day 1 to Day 3 and again at Day 5/6. Overall, there was an
187 increase in the CSL cells versus live cells at Day 6 in all three chemotherapy groups (Fig. 3B). The
188 overall viability continuously decreased each day following all three chemotherapy treatments, while
189 belinostat further reduced viability compared to control from Day 4 to Day 6 (Fig. 3B), indicating an
190 increase in cytotoxicity with belinostat treatment in addition to its CSL reversal effect. Importantly,
191 belinostat reversed the upward trajectory of ALDH (Fig. S4A), CSL cells versus live cells (Fig. 3B), and
192 CSL cells versus total cells (Fig. S4A) with a significant reduction in treated versus control at Day 6. Of
193 note, CD44 was only reversed by belinostat following carboplatin and paclitaxel treatments, but not
194 doxorubicin treatment (Fig. S4A), suggesting some differences in chemotherapy effects. The FACS
195 analysis for ALDH and CD44 levels versus live cells at Day 0, Day 3, Day 5, and Day 6 with DMSO or
196 belinostat are detailed in Fig. S4B, and show the reduced viability and abundance of CSL cells versus live
197 cells following belinostat treatment with all three chemotherapies. Summarized results across

198 chemotherapy treatments show a statistically significant reduction in ALDH+, CSL cells versus live cells,
199 CSL cells versus total cells, and viability with belinostat treatment at Day 6 (Fig. 3B and Fig. 4A).

200 Less consistent results were found in MDA-MB-231, a TNBC cell line (Fig. 3C and Fig. S5A).
201 CD44 (Fig. S5A), and CSL cells versus live cells (Fig. 3C) increased with doxorubicin and carboplatin,
202 but not paclitaxel. Further, CD44, CSL cells versus live cells, and CSL cells versus total cells (Fig. S5A)
203 all decreased with belinostat following chemotherapy treatments. Note, the reversal effect of belinostat on
204 ALDH was found upon paclitaxel treatment, but not doxorubicin or carboplatin (Fig. S5A). Detailed
205 FACS analysis for ALDH, CD44, and CSL cells versus live cells is also shown in Fig. S5B, and highlight
206 the reduced viability and abundance of CSL cells with belinostat treatment. Belinostat treatment exhibited
207 a statistically significant reduction across all chemotherapies in CD44, CSL cells versus live cells, CSL
208 cells versus total cells, and viability at Day 6 (Fig. S5A and Fig. 3C); however, ALDH levels were not
209 significantly different. Overall, the CSL reversal following chemotherapy was less pronounced in TNBC
210 than ER+ cells, perhaps reflecting higher baseline CSL in TNBC (23).

211 **Belinostat inhibits chemotherapy-derived CSL enrichment in ER+ patient tumor cells**

212 As chemotherapy strongly promoted CSL state in ER+ breast cancer patient samples, with a less
213 pronounced effect in TBNC patient samples as indicated above (Fig. 1B), we further tested the CSL
214 reversal effect of belinostat in ER+ patient cancer cells. These studies use patient samples to further test
215 the cell line results from above. Three ER+, PR+, Her2- breast cancer patient samples (Patient#5,
216 Patient#6, and Patient#7) were used to perform the same experiments as used for the cell lines. The
217 patient 3D organoids were treated with doxorubicin, carboplatin and paclitaxel for 72 hours respectively,
218 and followed by either control DMSO or belinostat (1μM or 2.5μM) for 72 hours. Relative fold changes
219 compared to DMSO control were expressed with curves for each individual patient sample treated with
220 three chemotherapies. As shown in Fig. S6A and Fig. 4A, FACS analysis of these cells show that ALDH
221 and CSL cells versus live cells were generally increased by chemotherapy and reversed by belinostat.

222 Note, CD44 decrease was found in the majority but not all of the patient cells (Fig. S6B). CSL cells
223 versus total cells were reduced by belinostat in the patient samples, although induction of CSL state alter
224 chemotherapy varied by patient, most likely due to prior treatments the patient received and various levels
225 of response to chemotherapy (Fig. S6C). Importantly, we found all chemotherapies decreased the viability
226 of cancer cell, and belinostat further decreased viability in a dose-dependent manner (Fig.4B). Across all
227 patient samples, FACS analysis showed increases in ALDH (Fig. S6D), CSL cells versus live cells (Fig.
228 4C), and CSL cells versus total cells (Fig. S6E) following chemotherapy treatment compared to vehicle
229 controls, and all are significantly decreased by belinostat in dose-dependent manner compared to
230 chemotherapy treatment only controls. Note, CD44 levels did not show a significant common effect either
231 on chemotherapy promotion or belinostat reversal, although the expected trends could be observed
232 between indicated groups (Fig. S6F). The viability decreased with all chemotherapies, and further
233 decreased with belinostat in dose-dependent manner (Fig. 4D). Overall, these experiments validated the
234 cell line studies with patient tumor samples and show that belinostat may serve as a general anti-CSL
235 inhibitor following multiple chemotherapies in ER+ breast cancer, reflecting a one-two punch treatment
236 strategy.

237 **Belinostat inhibits chemotherapy induced mammosphere formation**

238 We next tested the ability of belinostat to modulate CSL self-renewal and proliferation using a
239 mammosphere formation assay (24). Two cycles of mammosphere culture were performed to select stem-
240 like cells with self-renewal ability and eliminate various transitions following chemotherapy +/-
241 belinostat. Both CAMA-1 and MDA-MB-231 cells show a significantly diminished mammosphere
242 formation following belinostat treatment after chemotherapy after two-cycle cultures (Fig. 5A, B, C, D).
243 The majorities of chemotherapies increased the total mammosphere numbers and areas compared to
244 DMSO control only, while belinostat decreased the total mammosphere counts as well as their areas
245 compared to the chemotherapy plus DMSO control.

246 For the ER+ cells, doxorubicin and paclitaxel both increased mammosphere counts (up to 174.1%
247 and 131.1%), and mammosphere total areas (up to 257.9% and 211.9%) compared to DMSO control (set
248 to 100% for each condition). Strikingly, belinostat dramatically reduced the mammosphere counts (to 2.9-
249 3.7%) and mammosphere total areas (to 2.3-6.7%) following all chemotherapy treatments. Similarly, for
250 the TNBC cells, all chemotherapies strongly increased mammosphere counts (up to 490.6%, 330.8%, and
251 353.8%), and mammosphere total areas (up to 736.2%, 320.8%, and 366.6%) compared to DMSO
252 control. Belinostat again reduced the mammosphere counts (42.7-51.3%) and mammosphere total areas
253 (21.5-71.9%) following all chemotherapy treatments. Thus, the general anti-CSL effect of belinostat is
254 supported by its ability to inhibit CSL self-renew and proliferation with mammosphere assays.

255 **MYC pathways mediated CSL promotion/reversal upon chemotherapy/belinostat treatment**

256 To understand how belinostat reverses the chemotherapy-induced CSL properties, we performed
257 single-cell RNA-Seq analysis with two ER+ patient samples (Patient#5 and Patient#6). We performed an
258 unbiased clustering of the gene expression profiles of the Patient#6 and Patient#5 cells and saw that there
259 are changes in the gene expression profiles of the cells after chemotherapy treatments and combination
260 chemotherapies plus belinostat (Fig. 6A, B). The Patient#6 cells exhibited relatively similar
261 transcriptional programs to all chemotherapies, and also to the combination treatments. Chemotherapy
262 generated a distinctive cell population that was further changed by chemo+belinostat treatment (Fig. 6A).
263 This indicates that, while we previously saw that belinostat can reverse the stem cell phenotypes, it does
264 not reverse all aspects of the chemotherapy. In contrast, the Patient#5 cells showed a drug-specific
265 response where each chemotherapy led to distinct changes in the cell populations, and relatively little
266 changes in the transcriptional programs were induced by belinostat (Fig. 6B) .

267 As belinostat can induce changes in the stem cell related markers (Fig 4), the lack of obvious
268 changes in the overall transcriptional profiles suggest that the differences in the stem cell program may
269 leave a relatively small imprint on the overall profiles or that progenitor cell transcriptional profiles are

270 more nuanced. To focus on the specific (rather than overall) changes seen with drug treatment, we
271 performed a pathway analysis to identify the pathways that are altered by chemotherapy or combination
272 treatment.

273 Shared reversal pathways were selected as described in Methods, and heat maps were generated
274 based on the averages of ssGSEA enrichment scores for the shared reversal pathways for both Patient#6
275 (Fig. S7A, B) and Patient#5 (Fig. S7C, D). For each patient sample, we selected the pathways that were
276 either increased by chemo and decreased by belinostat, or decrease by chemo and increased by belinostat
277 (Fig. S7). In our shared reversal pathways analysis, we found that HDAC pathways
278 (HELLER_HDAC_TARGETS_DN) were up-regulated by all three chemotherapy treatments in both
279 patient samples and down-regulated by belinostat except paclitaxel group in Patient#6 (Fig. 6C, D). This
280 indicates that chemotherapy treatments promoted HDAC targets in this gene set (eg, CD44 as stemness
281 marker, BCL2 as anti-apoptotic regulator), while belinostat, a pan-HDAC inhibitor (HDACi), reversed
282 them; concomitant with the changes in CSL properties. This is consistent with prior reports showing that
283 HDAC expression is up-regulated in CSCs (13) and HDAC inhibitors can inhibit CSL phenotypes
284 through its inhibition of acetylation activity (13, 14).

285 We also observed that a stem cell differentiation signature
286 (BOQUEST_STEM_CELL_CULTURED_VS_FRESH_UP) was reduced by all three chemotherapy
287 treatments and promoted by belinostat in both patient samples (Fig. 6C, D). In another words, the CSL
288 state of the survival single cells were up-regulated by all chemotherapy treatments, and down-regulated
289 by belinostat. Consistent with CSL state, the MYC pathway (BILD_MYC_ONCOGENIC_SIGNATURE)
290 was increased by most of chemotherapy treatments, and inhibited by belinostat except paclitaxel group in
291 both Patient#6 (Fig. 6C) and Patient#5 (Fig. 6D). Belinostat has been reported to regulate MYC
292 expression transcriptionally and post-transcriptionally through regulation of MYC acetylation (25). MYC
293 has previously been shown to be a factor in CSC reprogramming and self-renewal in basal-like breast

294 cancer (26), and may contribute to reversal of the CSL promotion-reversal process mediated by
295 chemotherapy and HDACi.

296

297 **Discussion**

298 Cancer stem cells (CSCs) have the capacity to initiate growth of new tumors as well as cause
299 disease relapse; further, these cells are not targeted by conventional chemotherapy or other treatment
300 strategies (27). Therefore, there remains potential in developing treatment approaches that minimize CSC
301 or CSL cells to delay or prevent refractory cancer development. Our study indicates that subclonal
302 selection in patients during therapy promotes CSL state in breast cancer. Further, both flow cytometry
303 and mammosphere assays show a reversal of CSL state following chemotherapy by the use of the HDAC
304 inhibitor belinostat. Single-cell RNA sequencing analysis indicated that the RNA transcriptome was
305 strongly reprogramed by chemotherapy treatments, and reversed by belinostat, which promoted stem cell
306 differentiation, and inhibited HDAC targets and MYC pathway. The imbalance between acetylation and
307 deacetylation of histone or non-histone proteins, which are regulated by histone acetyltransferases
308 (HATs) and deacetylases (HDACs), have been proved closely to be associated with cancer development
309 (28). Acetylation and deacetylation of proteins is involved in various stemness-related signal pathways
310 and can regulate self-renewal and differentiation signaling (28). The pan HDAC inhibitor used in this
311 study have been used previously for their anti-tumor and anti-CSC activity by targeting multiple signaling
312 pathways at different molecular levels (14, 29). Besides chromatin remodeling via histone acetylation,
313 HDAC inhibitors could also block key signaling pathways pertinent to CSC maintenance, including HIF-
314 1α, Stat3, Notch1, β-catenin, NF-κB, MYC, and c-Jun with the ability of different HDAC isoforms to
315 regulate protein stability and/or activity (14).

316 Although HDAC inhibitors have been used alone or in combination therapy to suppress the CSC
317 population in different settings (14), how HDAC inhibitors reverse CSL state following standard of care

318 chemotherapies is not well-defined. Previous clinical trials of HDACi target to CSL cells either focused
319 on the monotherapy for refractory peripheral T-cell lymphoma, or concurrent combination of
320 chemotherapy with HDACi on solid tumors (Poole 2014). However, these clinical trials and research
321 assessed antitumor activity by apoptosis/viability test, more than targeting to acquired stemness. In
322 addition, it has not been studied if specific chemotherapies, or this class of drug generally, can induce
323 CSL state. Further, it has not been studied if HDAC inhibitors can reverse CSL states driven by different
324 chemotherapies. As detailed results above, our study addresses subclonal evolution of stem-like traits in
325 patients as they acquire resistance to chemotherapy, as well as approaches to reverse this acquired
326 resistant trait.

327 In this study, we initially tested multiple drugs published previously to block stem cell-like state.
328 Only one was effective following chemotherapy induced stem-like states across cell lines and patient
329 tumor cells. Although there was some heterogeneity in ALDH or CD44 expression level modulated by
330 different chemotherapies, we generally saw an increase in CSL levels for ER+ tumor cells and to a lesser
331 extent TNBC cells. Belinostat broadly blocked increased CSL cells following chemotherapy treatment
332 based on flow cytometry and mammosphere assays. However, entinostat, another HADC inhibitor target
333 to HDAC1 and HDAC3, did not exhibit the general reversal effect (Fig. 2), although additional
334 cytotoxicity was found when given after chemotherapy, which might suggest specific HDAC isoform(s)
335 could be responsible to this general CSL state reversal. This question could be further determined in the
336 future work. Although HDAC inhibitors have been proved for their epigenetic effect on the
337 reprogramming of gene expression in cancer cells, which leads to growth arrest, differentiation, and
338 apoptosis (30), their roles in suppressing the self-renewal capability and driving the differentiation of
339 CSCs could also enhance the cancer cell sensitivity to chemotherapy (Liu et al., 2017), which might lead
340 a synergistic effect for CSL elimination. HDAC inhibitors also prevent or reverse the development of
341 drug resistance by its inhibition on drug transporters (MDR1) expression, thus augmenting the effect of
342 combined therapy with their synergism (31). The mammosphere formation assays in our study

343 demonstrated that belinostat could abolish the self-renewal capability of survival cells after chemotherapy
344 treatments, which has resulted in resistant CSL subtypes. Importantly, these results were consistent across
345 different chemotherapies tested, suggesting a convergence on CSL resistance. The synergistic effects of
346 these drug combinations as well as optimal timing and sequence should be determined by further
347 experiments and mathematical modeling.

348 In our FACS strategy to identify the CSL cells, ALDH and CD44 were selected as the CSL state
349 markers, rather than CD24. Of Note, the initial state of CAMA-1 starts from very low primitive cell traits
350 (indicated by low CD44 level) compared to MDA-MB-231, which might suggests more potential for CSL
351 state induction for ER+ cells other than TNBC. Recently, two types of distinct CSCs, epithelial-like (E)
352 ALDH+ CSCs and mesenchymal-like (M) CD44+/CD24− CSCs, have been identified (Sulaiman et al.,
353 2019). Liu et al reported that E and M CSCs co-existed in all breast cancer subtypes, but their proportions
354 were varied (32). ALDH+ CSCs located within the core of the tumor with high expression of E-cadherin
355 but low expression of vimentin and ZEB1, undergo proliferation at hypoxia conduction, while
356 CD44+/CD24− CSCs located at the edge of the breast tumor with low expression of E-cadherin but high
357 expression of vimentin and ZEB1, undergo migration and invasion (32). These two subtypes of CSCs
358 exhibit differential signal pathway regulations, plasticity, and differently responses to treatment. E and M
359 CSCs were also found to be interconvertible in EMT-MET signaling. Therefore, co-inhibition of both E
360 and M subtypes of CSCs may be needed to develop effective therapy (L32). The detailed time-course
361 FACS analysis following chemotherapies (Fig. S4B, Fig. S5B) suggests belinostat potentially exhibited
362 dual inhibition of E and M CSL cells, with its reversal effect mainly on CD44 in TNBC cell line MDA-
363 MB-231 (initially ALDH low/CD44 high), which is enriched with M subtype of CSL cells (23), and on
364 ALDH in ER+ cell line CAMA-1 (initially ALDH high/CD44 low) and patient samples, which is
365 enriched with E subtype of CSL cells. Compared to the FACS analysis for CSL state, the mammosphere
366 assay tests the self-renewal ability of resistant cells rather than the changes of stemness makers. Cells
367 with high level expression of CD44 are more resistant to chemotherapy and likely to form mammosphere

368 (23), which would benefit the TNBC than ER+ cells due to their enrichment of progenitor cells (ALDH
369 negative, CD44 high). In this case, inhibition effect of belinostat on CD44+ cells could play a major role
370 to abolish the self-renewal capability of chemo-resistant cells. Reversal of CD44 in ER+ cell lines/patient
371 samples and Inhibition of ALDH in TNBC cell line were also identified by FACS analysis, which varied
372 among cell lines/patient samples with different chemotherapies. Thus, future research may help delineate
373 cell populations sensitive to belinostat treatment.

374 In the single-cell RNA sequencing analysis, we are interested in visualizing the pattern of
375 activation of the pathways across the different treatment groups, other than seeking the overall changes by
376 leveraging multiple pairwise comparisons against control treated cells and then plotting the enrichment
377 score or a metric based on the statistical significance. The approach we used could more directly provide
378 information such as the relative magnitude of the changes, as well as the baseline levels of activation in
379 the control group. In the single-cell RNA sequencing analysis presented here, chemotherapy followed by
380 belinostat revealed that MYC could be an important mediator for these two distinct subtypes of CSCs.
381 MYC induces the dedifferentiation towards a progenitor-like state by epigenetic reprogramming (Yoshida
382 et al., 2018). Further, mammosphere with MYC overexpression showed enrichment for cells expressing
383 ALDH1 (34). MYC-dependent metabolic reprogramming is related to CD44 variant-dependent redox
384 stress regulation in CSCs (33). Targeting MYC family by HDAC inhibition, such as valproic acid, could
385 contribute to the down-regulation of MYC, in turn to up-regulate of CDKN1A/B (p21/CIP1/WAF1,
386 p27/KIP1) to induce cell cycle arrest and autophagic cell death (33, 35).

387 The patient data described in this study supports the model that tumor subclones with enrichment
388 of a CSL phenotype are selected during acquisition of a drug resistant state. It remains unclear how the
389 genetic composition of tumor subclones impacts phenotype. The CNVs used to identify these survivor
390 subclones harbor numerous genes, which may combine to enhance plasticity or a CSL state. This question
391 could be further elucidated in future studies with a larger sample size.

392 Taken together, our findings demonstrated HDAC inhibition reverses chemotherapy-induced
393 acquisition of primitive cell traits and drug-resistance in ER+ breast cancer, and provided an effective
394 'one-two punch' strategy to combat refractory ER+ breast cancer with sequential chemotherapy and
395 HDACi combination.

396

397 **Materials and Methods**

398 Human subjects

399 Informed consent was obtained from all patients in this study. Protocols were approved by the University
400 of Utah Institutional Review Board and the City of Hope Institutional Review Board.

401

402 Cells and drugs

403 Breast cancer cell lines CAMA-1, T47D, MCF7, ZR-75-1, MDA-MB-231, BT549, HCC38, HCC1143,
404 and HCC1395 were all obtained from ATCC. The following drugs were selected as the potential CSL
405 inhibitors as shown in Table 1, which includes AXL inhibitors (BGB324 and TP-0903), Wnt/CBP
406 inhibitor (ICG-001,), Hedgehog inhibitor (vismodegib), CDK8 inhibitor (SenexinA), CDK4/6 inhibitor
407 (Ribociclib and Abemaciclib), HDAC inhibitors (Belinostat and Entinostat), FGFR inhibitor (AZD4547),
408 EGFR inhibitors (Afatiniband Gefitinib), and ALDH inhibitor (Disulfiram, DSF). BGB324 was obtained
409 from BerGenBio. All other inhibitors mentioned above and chemotherapy drugs (Doxorubicin,
410 Carboplatin, and Paclitaxel) were purchased from Selleckchem.

411

412 Sample collection

413 Primary breast cancer samples were obtained from malignant pleural effusions or ascites. Patients #1-4,
414 #7-8, #11 are from pleural effusions, patient #5-6, #9-10, #12 are from ascites. After fluid drainage, cells
415 were pelleted at 300 × g for 5 min, and resuspended in TAC buffer (17mM Tris, pH 7.4, and 135mM

416 NH4Cl), followed with incubation at 37 °C for 5 min and centrifugation. After repeating these steps
417 several times until red blood cells were completely depleted from pellet, the remaining cells were washed
418 with PBS twice and frozen in 90% FBS with 10% dimethyl sulfoxide (DMSO).
419
420 Treatment of patient cultures/breast cancer cell lines with chemotherapy and CSL inhibitors for FACs
421 analysis
422 For patient samples used for FACS analysis and single cell RNA sequencing, we thawed frozen viable
423 breast cancer pleural effusions or ascites from patients and depleted dead cells with EasySep™ Dead Cell
424 Removal (Annexin V) Kit (STEMCELL Technologies) and CD45+ cells with EasySep™ Human CD45
425 Depletion Kit II (STEMCELL Technologies) according to manufacturer protocols. These purified cancer
426 cells were then resuspended in Renaissance Essential Tumor Medium (RETM, Cellaria) containing 5%
427 FBS, RETM supplement, antibiotic/antimycotic (anti-anti), and 20 ng/mL cholera toxin. For
428 chemotherapy dose response evaluation, patient cells were counted and plated at 10,000 per well in 100
429 μL RETM with 96-well spheroid plates with black walls (Corning 4520). Breast cancer cell lines were
430 counted and plated at 40,000 per well in 100 μL culture medium (RPMI contain 10% FBS, 1% antibiotic-
431 antimycotic for T47D, ZR-75-1, MDA-MB-231, BT549, HCC38, HCC1143, and HCC1395, DMEM
432 containing 10% FBS, 1% antibiotic-antimycotic for CAMA-1 and MCF7). After 18-24 hours, 100 μL
433 culture medium with drug (2X dose) was added. Cells were harvested after 72 hours for ALDEFLUOR
434 and CD44 staining and FACS. For CSL inhibitor treatment, cells were plated and treated with
435 chemotherapy the same as mentioned above. After 72 hours, the medium was removed, and the
436 organoids were washed with fresh medium once and replaced with 200 μL fresh medium containing CSL
437 inhibitors. The cells were harvested after another 72 hours incubation for ALDEFLUOR and CD44
438 staining and FACS.
439
440 Flow Cytometry

441 The organoids were collected by centrifugation at 300g for 5min, and dissociated with trypsin-EDTA for
442 5min at 37°C. The cells were incubated with ALDEFLUOR staining (STEMCELL TECHNOLOGIES)
443 for 30 minutes at 37°C, and then anti-CD44-PE antibody (1:50 Miltenyi) for 25 minutes on ice in
444 ALDEFLUOR Assay Buffer according to the protocol. The samples with DEAB inhibitor without CD44-
445 PE staining serve as the negative control for ALDEFLUOR. For chemo dose response evaluation and
446 CSL inhibitor screening, each sample takes 200 μL /mL for ALDEFLUOR Assay and 100 μL
447 ALDEFLUOR Assay Buffer for CD44 staining. DAPI (1 μg/mL for final concentration) was added to
448 label the dead cells before FACS test.
449
450 Mammosphere Assay
451 Mammosphere Assay was performed following the protocol mentioned in Shaw L et al with modification
452 (Shaw et al., 2012). Cells were plated in 96-well spheroid plates with black walls (Corning 4520) at
453 40,000 per/well in 100μL medium. After 18-24 hours, another 100μL medium with 2x drug was added
454 (final concentration Doxorubicin 0.1μM, Carboplatin 50μM, Paclitaxel 1μM). After 72 hours, the
455 spheroids were harvested from 24 wells, and dissociated with Trypsin for 5min at 37°C. The cells were
456 pelleted and resuspended in 1mL mammosphere media (500mL phenol-free RPMI plus 20mL B27, plus
457 rEGF 20ng/mL). For each treatment, the cells were seeded at 18000/well in 6 well plates (ultralow
458 attachment from Corning #3471) with 2mL media supplied with DMSO or Belinostat 5μM in triplicates.
459 After 14 days in culture, the mammospheres were imaged with a Zeiss Axio Observer 7 microscope from
460 triplicate wells. For the second mammosphere culture, the mammospheres from the same treatment were
461 collected and incubated with Trypsin for 5min at 37°C, followed by 10 passages through a 22 gauge
462 needle for dislocation. The cells were seeded again at 18000/well in 6 well ultralow attachment plate with
463 2mL media supplied with DMSO or Belinostat 5μM in triplicates as the same conditions in the first
464 mammosphere culture. After another 14 days in culture, the mammospheres were imaged again with a
465 Zeiss Axio Observer 7 microscope from triplicate wells. All the mammospheres were counted using
466 Qupath software (a length greater than 80 μm) for both number and area.

467

468 CNV analysis

469 CNV analysis of four patients' pre- and post-treatment WGS or WES data were performed and subclonal
470 CNVs were identified as described previously (Brady et al., 2017). Briefly, somatic CNVs between
471 integer copy values were considered to be subclonal, such that a region with average CNV 2.5 pre-
472 treatment and which became 3.0 post-treatment was considered to be a mixture of 50% 2-copy cells and
473 50% 3-copy cells in the pre-treatment sample. For tumor, the Bulk WGS sequencing coverage to identify
474 subclonal CNAs for Patient #1-4 are 60X, 60X, 40X, and 60X, respectively. For germline, the bulk WGS
475 sequencing coverage for Patient #1-4 are 60X, 60X, 40X, and 40X, respectively. For Selecting copy
476 number changes, certain copy number variants were selected by analyzing subclonal, non-integer copy
477 number variants. Other regions do not contribute to this assessment; for example, please reference the
478 horizontal dotted lines along the integer values (at 1, 2, 3, 4, etc.) in S1D-G, which show that copy
479 number variants at these integer positions are not necessary for these analyses. For Stem WGS coverage
480 (1-10X estimated) for comparing subclonal CNA levels between stem cell populations, Low-pass
481 sequencing coverage was used for the ALDH/CD44 sorting for all four patients, with approximately 4X
482 coverage for each sample. The sequencing coverage for Patient #1-4 are 3.3X, 2.5X, 2.5X, and 3.3X,
483 respectively. As shown in Fig. S1D, the therapy-resistant subclones in Patient#1 demonstrated CNVs on
484 chromosomes 3, 4, and 9, whereas therapy-responsive subclones had CNVs on 12, 14, and 16; Patient#2
485 had responsive CNVs on chromosomes 7q and 11q (Fig. S1E); Patient#3 had resistant CNVs on
486 chromosomes 6 and 7 and a responsive CNV on chromosome (Fig. S1F); and Patient#4 had a resistant (or
487 at least increasing) CNV on chromosome 4 (Fig. S1G). Note that Patient#4's chromosome 4 amplification
488 does not appear to have changed after treatment, but in fact, increased in the tumor cell population
489 because the sample has much more normal contamination with only ~25% tumor purity (Fig. S1F).

490 CSL proportion calculation in each subclone

491 To identify CNVs from CSL (ALDH+/CD44+) vs. non-CSL populations, we thawed frozen viable breast
492 cancer pleural effusions or ascites from patients and depleted normal cells, including white blood cells
493 (CD45+), fibroblasts (CD90+), and mesothelial cells (podoplanin+) using the Miltenyi BioTec
494 quadroMACS system with the following protocol. Four mL of quadroMACS buffer (cold PBS with 0.5%
495 BSA and 2 mM EDTA) was added to cells and cells were spun down at 1000 g for 5 minutes at 4 °C.
496 Cells were resuspended in 1 mL quadroMACS buffer, and 10 µL of biotinylated anti-podoplanin antibody
497 (Biolegend #337015) was added. Cells were incubated 10 minutes on ice and spun down at 300 x g for 5
498 minutes at 4 °C to wash off excess antibody. Cells were resuspended in 120 µL quadroMACS buffer. To
499 this was then added 26 µL of anti-CD45 microbeads, 26 µL of anti-CD90 microbeads, and 26 µL of anti-
500 biotin microbeads (Miltenyi BioTec). Cells were incubated 15 minutes on ice in the dark, followed by
501 addition of 1 mL quadroMACS buffer and cells were then spun down 300 x g for 5 minutes at 4 °C. Cells
502 were resuspended in 500 µL quadroMACS buffer, then added to pre-washed (with 2 mL quadroMACS
503 buffer) LD column, and elute was collected. One mL quadroMACS buffer was added to column and elute
504 continued to be collected; this was repeated an additional time for a final elute volume of 2.5 mL. Cells
505 were then spun down at 1000 g for 5 minutes at 4 °C. We then stained purified breast cancer cells using
506 the ALDEFLUOR system according to manufacturer's instructions to assess ALDH activity, followed by
507 staining with a CD44-PE antibody in ALDEFLUOR assay buffer for approximately 30 minutes on ice.
508 Cells were washed in ALDEFLUOR assay buffer followed by FACS to assess the number of cells which
509 were ALDH+/CD44+, ALDH+/CD44-, ALDH-, CD44+, or ALDH-/CD44- (referred to as quadrants
510 hereafter), and to sort cells in order to isolate genomic DNA from each of these four populations. Isolated
511 genomic DNA was then sequenced by Illumina whole-genome sequencing at low coverage (2X to 10X)
512 to infer CNVs. To infer CNVs, reads were aligned to hg19 using BWA using the Speed-Seq suite. Then
513 samtools pileup was run on the resulting aligned bam files, and the coverage in 1 million bins across the
514 genome was calculated and manually centered at absolute copy 2 (diploid). The percent of each subclone
515 in each quadrant could be calculated following the example below. An example analysis is shown in Fig.
516 S1B, where a non-stem population (ALDH-/CD44-) had ~1.6 copies of a chromosome 3 region (40% of

517 cells with chr3 deletion). Meanwhile, the CSL population (ALDH+/CD44+) had ~1.3 copies of this
518 region (70% of cells with chr3 deletion). Thus, the CSL population is enriched for cells with the chr3
519 deletion, and these cells represent the survivor subclone. To calculate the percent of each quadrant (CSL
520 population) in each subclone, the survivor subclone and the non-survivor subclones for CSL content are
521 converted following the example below. The number of cells in each stem quadrant (the number of cells
522 for DNA isolation) was recorded to make this conversion. The conversion could be performed like
523 following example described. Suppose the following numbers from FACS in each quadrant were
524 obtained:

525 1,000 ALDH+/CD44+ cells (CSL cells)

526 2,000 ALDH+/CD44- cells

527 2,000 ALDH-/CD44+ cells

528 10,000 ALDH-/CD44- cells (double-negative)

529 15,000 cells total

530 Then assume there were 20% of cells with a subclonal CNV (dubbed CNV-X) in the double-negative
531 non-stem population, but 50% of cells with CNV-X in the CSL population. Based on this, the absolute
532 number of CSL cells with the CNV-X is 1,000 * 0.5 = 500 cells. The absolute number of double-negative
533 cells with CNV-X would be 10,000 * 0.2 = 2,000 cells. This calculation could be performed for each
534 quadrant/subclonal-CNV pair, to get the absolute number of cells in each CSL quadrant for each
535 subclone. Then we sum the total cell number in each subclone in all four quadrants, and calculate the
536 percentage of cells in that subclone that are in each quadrant, with the sum total just described as the
537 denominator. This results in the CSL proportions of each subclone, as shown in Fig. 1A.

538

539 Single-cell RNA sample preparation and sequencing analysis

540

541 Staining of single cell suspensions for scRNA-Seq

542 The patient cells were isolated, cultured, and treated with chemotherapy +/- belinostat as methods
543 mentioned above for CSL inhibitor screening with FACs analysis. Cell organoids were collected by
544 centrifugation at 300g for 5min, and dissociated with trypsin-EDTA for 5min at 37°C. Dead cells were
545 depleted with EasySepTM Dead Cell Removal (Annexin V) Kit (STEMCELL Technologies, #17899).
546 Cells in suspension were stained with ReadyProbes Cell Viability Imaging Kit (Hoechst 33342 and
547 Propidium Iodide, Thermo Fisher Scientific) by adding 80µL each dye at 500,000 cell/mL in basal
548 DMEM medium and incubated for 20 minutes at 37°C + 5% CO2. After incubation, cells were diluted
549 with equal volume of 1X PBS (no Ca2+/Mg2+, pH 7.4, Thermo Fisher Scientific) then centrifuged for 5
550 minutes at 300 x g, 4°C. Cells were resuspended to $5.0x10^5$ to $2.0x10^6$ cell/mL in 1X PBS and calculated
551 concentrations on a hemocytometer using trypan blue then diluted to 50,000 cell/mL in 1x PBS +
552 0.2U/µL Superase· In RNase inhibitor (Thermo Fisher Scientific) + 1X Second Diluent (Takara Bio).
553
554 Single Cell Dispensing, Imaging, and Candidate Selection
555 Single-cell RNA-Sequencing (scRNA-Seq) was performed using the ICELL8® Single-Cell System
556 (Takara Bio) using the SMARTer™ ICELL8 3' DE Kit (Takara Bio). Processing 8 samples at a time,
557 80µL of each 50,000 cell/mL cell sample, negative control, positive control (K-562 RNA), and fiducial
558 reagent (dye control) were loaded into each well of a 384-well plate (A1 through D2) and dispensed 50nL
559 per well into a 5,184 well SMARTer™ ICELL8® 3' DE Chip (Takara Bio) using the ICELL8®
560 Multisample NanoDispenser (MSND, Takara Bio). After dispense, chip was sealed with imaging film,
561 and centrifuged at 300 x g, 5 minutes, 4°C. ICELL8® 3' DE Chip was then imaged on an ICELL8®
562 Imaging System (Takara Bio) featuring an Olympus BX43 upright florescent microscope equipped with
563 an automated stage, camera, DAPI, and Texas Red filters and controlled by CellSelect® Software (Takara
564 Bio) to visually identify and select wells containing one viable single-cell candidate per well (positive
565 Hoechst 33342, negative Propidium Iodide) generating single-cell candidate list for each ICELL8® 3' DE
566 Chip. After imaging, ICELL8® 3' DE Chip were stored at -80°C overnight. Each sample was ran twice
567 on separate ICELL8® 3' DE Chips in order to multiplex samples and minimize chip-to-chip variations.

568

569 RT-PCR, Library Construction, and Next Generation Sequencing

570 The ICELL8® 3' DE Chip is preprinted with a reverse transcription (RT) primer containing a unique
571 molecular identifier (UMI), 11-base unique well barcode, and poly T sequence in each of the 5,184 wells.
572 The ICELL8® 3' DE Chip containing cells was thawed at room temperature for 10 minutes, then
573 centrifuged for 3 minutes, 3,200 x g, 4°C and maintained on ice. The ICELL8® 3' DE Chip was placed
574 on the ICELL8® MSND and loaded 50 µL of RT-PCR solution (Takara Bio; 56 µL 5M GC Melt, 24 µL
575 25mM dNTP Mix, 3µL 1M MgCl2, 9µL 100mM DTT, 62 µL 5X First-Strand Buffer, 33 µL 2X SeqAmp
576 PCR Buffer, 16 µL 10% Triton X-100, 2 µL SMARTer ICELL8 3' DE Oligo Mix, 29 µL 100U/µL
577 SMARTScribe Reverse Transcriptase, 10µL SeqAMP DNA Polymerase) into four wells (A1 through A4)
578 of a 384-well plate. MSND then dispensed 50 nL to wells containing only live single-cell candidates
579 according to the single-cell candidate file previously generated by the ICELL8® Imaging System. The 3'
580 DE Chip containing single cell candidates with RT-PCR reagent sealed with PCR Sealing Film and
581 centrifuged 3,200 x g, 3 min, 4°C and then placed in a BioRad T100 equipped with a ICELL8® Chip
582 adapter to perform RT followed by 22 PCR cycles for cDNA amplification. Amplified cDNA from the
583 ICELL8® 3' DE Chip individual cells was collected and pooled using the ICELL8® Collection Kit
584 (Takara Bio) by centrifugation at 3,200 x g, 10 minutes, 4°C. The cDNA products were concentrated
585 using cDNA Clean & Concentrator-5 Kit (Zymo Research) followed bead cleanup using 0.6X AMPure
586 XP Beads (Beckman Coulter) and eluted in 12 µL DNase/RNase free water.

587 Libraries were prepared using 1ng of purified cDNA according to the ICELL8® 3' DE instruction manual
588 (Takara Bio) using the Nextera Primer P5 (ICELL8® 3' DE Kit, Takara Bio), Nextera XT DNA Library
589 Preparation Kit (Illumina) and i7 Index Primer (Nextera XT Index Kit, Illumina). Unique i7 Indexes were
590 used for each ICELL8® 3' DE Chip. Tagmented cDNA was amplified by PCR 12 cycles prior to dual-
591 sided bead cleanup using AMPure XP beads, and eluted in 11µL DNase/RNase free water. Library and
592 cDNA quality and profile were confirmed prior to sequencing ran on an Agilent Bioanalyzer using a

593 Bioanalyzer High Sensitivity DNA Analysis kit (Agilent). Prepared library was then sequenced using
594 150 paired-end cycles on a NovaSeq S4 flow cell (Illumina).
595
596 Single-cell RNA-Seq Analyses
597 Libraries were sequenced on an Illumina HiSeq 2500 with 2 X 125 paired-end reads. Raw FASTQ
598 sequencing files were processed by the Cell Ranger Single Cell Software Suite for demultiplexing,
599 barcode assignment, alignment and UMI counting (https://support.10xgenomics.com/single-cell-gene-
600 expression/software/overview/welcome). Samples were aligned to hg19 using the STAR aligner (36).
601 Count tables were generated with a total of 6196 cells for Patient#5 and Patient#6 and used as input into
602 Seurat v2 (37).
603
604 Quality control on the cells:
605 Low quality cells were filtered out if the library size was less than 10,000 or the number of expressed
606 genes (counts larger than 0) is less than 500. Furthermore, the cells with more than 30% mitochondrial
607 gene counts were discarded. For Patient#6, 3668 cells were acquired before filtering, 2773 cells were
608 acquired after filtering. For Patient#5, 2528 cells were acquired before filtering, and 1553 cells were
609 acquired after filtering.
610
611 Dimensionality reduction, clustering and visualization using UMAP
612 The Bioinformatics ExperT SYstem (BETSY) (38) was applied to cluster and visualize the scRNA-seq
613 data using UMAP. In short, an RNA-Seq count matrix was normalized to log scale with a scale
614 parameter of 10,000. Top 500 highly variable genes were then identified in the normalized dataset. The
615 linear dimensional reduction method PCA was then performed upon these variable genes. The first 10
616 principal components (PCs) and a resolution of 0.6 were used for Louvain graph-based clustering and
617 two-dimensional visualization with UMAP.
618

619 Pathway analysis

620 To identify the pathways reversed by belinostat that are shared by the three chemotherapy groups, we
621 applied the Single Sample Gene Set Enrichment Analysis (ssGSEA) by running the "ssGSEA" function
622 implemented in the GSVA package (v1.22.4) (39) in R (v3.4.3). The gene sets from the hallmark, C2 and
623 C6 collections of the Molecular Signatures Database (v6.2) were used for the ssGSEA. The
624 chemotherapy-belinostat reversal pathways shared among chemotherapy groups were selected with the
625 following steps. Student T-test between chemo+DMSO vs. DMSO+DMSO and chemo+belinostat vs.
626 chemo+DMSO were performed with all ssGSEA enrichment scores for single cells within each
627 chemotherapy group, and all the GSEA pathways with significant adjusted p value ($p<0.05$) in both T-
628 tests were selected. GSEA pathways with reversal directions in two T-test groups were indicated by the
629 reversal log2 fold changes in the enrichment scores, and filtered with the condition that the pathways
630 must be shared by at least two chemotherapy groups with the same trends. The averaged enrichment
631 scores across all cells in each treatment group were used as the input data to generate heat maps.

632

633 Statistical Analysis

634 For Single-cell RNA sequencing analysis, the R packages "stats" and "rstatix" were used to perform
635 statistical tests. Student's t-test (two-tailed) was used to compare the Single Sample Gene Set Enrichment
636 Analysis (ssGSEA) scores between two treatment groups. α level was considered 0.05 for all statistical
637 tests. Error bars for all drug and inhibitor assays represent standard deviation of three replicates from one
638 assay. For all statistical analysis in experiments other than bioinformatics analysis, student's t-test (two-
639 tailed) was used between groups according to the description in the legends. For all FACS analysis and
640 mammosphere assays, student's t-tests were performed between treatments vs. controls as indicated in
641 figure legends with triplicate tests. Significance is marked with * for $P<0.05$, ** for $P<0.01$, *** for
642 $P<0.001$.

643

644

645

646 **References and Notes**

647 1. A. M. Gonzalez-Angulo, F. Morales-Vasquez, G. N. Hortobagyi. Overview of resistance to
648 systemic therapy in patients with breast cancer. Adv. Exp. Med. Biol. 608, 1–22 (2007).
649 2. V. Malhotra, M. C. Perry. Classical chemotherapy: mechanisms, toxicities and the therapeutic
650 window. Cancer Biol. Ther. 2, S2–4 (2003).
651 3. B. A. Chabner, T. G. Jr. Roberts. Timeline: Chemotherapy and the war on cancer. Nat. Rev.
652 Cancer. 5, 65–72 (2005).
653 4. D. X. Nguyen, P.D. Bos, J. Massague. Metastasis: From dissemination to organ-specific
654 colonization. Nat. Rev. Cancer. 9, 274–284 (2009).
655 5. P. Valent, D. Bonnet, R. De Maria, T. Lapidot, M. Copland, J. V. Melo, C. Chomienne, F.
656 Ishikawa, J. J. Schuringa, G. Stassi, B. Huntly, H. Herrmann, J. Soulier, A. Roesch, G. J.
657 Schuurhuis, S. Wöhrer, M. Arock, J. Zuber, S. Cerny-Reiterer, H. E. Johnsen, M. Andreeff, C.
658 Eaves. Cancer stem cell definitions and terminology: the devil is in the details. Nat. Rev. Cancer.
659 12, 767–775 (2012).
660 6. M. Al-Hajj, M. S. Wicha, A. Benito-Hernandez, S. J. Morrison, M. F. Clarke. Prospective
661 identification of tumorigenic breast cancer cells. Proc. Natl. Acad. Sci. U. S. A. 100, 3983-3938
662 (2003).
663 7. S. Palomeras, S. Ruiz-Martínez, T. Puig. Targeting Breast Cancer Stem Cells to Overcome
664 Treatment Resistance. Molecules. 23, E2193 (2018).
665 8. Y. Lombardo, A. de Giorgio, C. R. Coombes, J. Stebbing, L. Castellano. Mammosphere
666 formation assay from human breast cancer tissues and cell lines. J. Vis. Exp. 97 (2015).
667 9. Y. A. Luqmani. Mechanisms of drug resistance in cancer chemotherapy. Med. Princ. Pract. 14,
668 35-48 (2005).

669 10. G. Chu. Cellular responses to cisplatin. The roles of DNA-binding proteins and DNA repair. J.
670 Biol. Chem. 269, 787–790 (1994).
671 11. C. J. Creighton, X. Li, M. Landis, J. M. Dixon, V. M. Neumeister, A. Sjolund, D. L. Rimm, H.
672 Wong, A. Rodriguez, J. I. Herschkowitz, C. Fan, X. Zhang, X. He, A. Pavlick, M. C. Gutierrez,
673 L. Renshaw, A. A. Larionov, D. Faratian, S. G. Hilsenbeck, C. M. Perou, M. T. Lewis, J. M.
674 Rosen, J. C. Chang. Residual breast cancers after conventional therapy display mesenchymal as
675 well as tumor-initiating features. Proc. Natl. Acad. Sci. U. S. A. 106, 13820–13825 (2009).
676 12. F. H. Groenendijk, R. Bernards. Drug resistance to targeted therapies: Deja vu all over again.
677 Mol. Oncol. 8, 1067–1083 (2014).
678 13. M. R. Doherty, J. M. Smigiel, D. J. Junk, M. W. Jackson. Cancer Stem Cell Plasticity Drives
679 Therapeutic Resistance. Cancers (Basel) 8, E8 (2016).
680 14. P. C. Lin, H. Y. Hsieh, P. C. Chu, C. S. Chen. Therapeutic Opportunities of Targeting Histone
681 Deacetylase Isoforms to Eradicate Cancer Stem Cells. Int. J. Mol. Sci. 19, pii: E1939 (2018).
682 15. S. V. Sharma, D. Y. Lee, B. Li, M. P. Quinlan, F. Takahashi, S. Maheswaran, U. McDermott, N.
683 Azizian, L. Zou, M. A. Fischbach, K. K. Wong, K. Brandstetter, B. Wittner, S. Ramaswamy, M.
684 Classon, J. Settleman. A chromatin-mediated reversible drug-tolerant state in cancer cell
685 subpopulations. Cell. 141, 69-80 (2010).
686 16. C. Kim, R. Gao, E. Sei, R. Brandt, J. Hartman, T. Hatschek, N. Crosetto, T. Foukakis, N. E.
687 Navin. Chemoresistance Evolution in Triple-Negative Breast Cancer Delineated by Single-Cell
688 Sequencing. Cell. 173, 879-893 (2018).
689 17. N. Sachs, J. de Ligt, O. Kopper, E. Gogola, G. Bounova, F. Weeber, A. V. Balgobind, K. Wind,
690 A. Gracanin, H. Begthel, J. Korving, R. van Boxtel, A. A. Duarte, D. Lelieveld, A. van Hoeck, R.
691 F. Ernst, F. Blokzijl, I. J. Nijman, M. Hoogstraat, M. van de Ven, D. A. Egan, V. Zinzalla, J.
692 Moll, S. F. Boj, E. E. Voest, L. Wessels, P. J. van Diest, S. Rottenberg, R. G. J. Vries, E. Cuppen,
693 H. Clevers. A Living Biobank of Breast Cancer Organoids Captures Disease Heterogeneity. Cell.
694 172, 373-386 (2018).

695 18. J. A. Colacino, E. Azizi, M. D. Brooks, R. Harouaka, S. Fouladdel, S. P. McDermott, M. Lee, D.
696 Hill, J. Madden, J. Boerner, M. L. Cote, M. A. Sartor, L. S. Rozek, M. S. Wicha. Heterogeneity
697 of Human Breast Stem and Progenitor Cells as Revealed by Transcriptional Profiling. Stem Cell
698 Reports. 10, 1596-1609 (2018).
699 19. S. W. Brady, J. A. McQuerry, Y. Qiao, S. R. Piccolo, G. Shrestha, D. F. Jenkins, R. M. Layer, B.
700 S. Pedersen, R. H. Miller, A. Esch, S. R. Selitsky, J. S. Parker, L. A. Anderson, B. K. Dalley, R.
701 E. Factor, C. B. Reddy, J. P. Boltax, D. Y. Li, P. J. Moos, J. W. Gray, L. M. Heiser, S. S. Buys,
702 A. L. Cohen, W. E. Johnson, A. R. Quinlan, G. Marth, T. L. Werner, A. H. Bild. Combating
703 subclonal evolution of resistant cancer phenotypes. Nat. Commun. 8, 1231 (2017).
704 20. S. Ricardo, A. F. Vieira, R. Gerhard, D. Leitão, R. Pinto, J. F. Cameselle-Teijeiro, F. Milanezi, F.
705 Schmitt, J. Paredes. Breast cancer stem cell markers CD44, CD24 and ALDH1: expression
706 distribution within intrinsic molecular subtype. J. Clin. Pathol. 64, 937-946 (2011).
707 21. E. Charafe-Jauffret, C. Ginestier, F. Iovino, J. Wicinski, N. Cervera, P. Finetti, M. H. Hur, M. E.
708 Diebel, F. Monville, J. Dutcher, M. Brown, P. Viens, L. Xerri, F. Bertucci, G. Stassi, G. Dontu,
709 D. Birnbaum, M. S. Wicha. Breast cancer cell lines contain functional cancer stem cells with
710 metastatic capacity and a distinct molecular signature. Cancer Res. 69, 1302-1313 (2009).
711 22. S. Lim, P. Kaldis. Cdks, cyclins and CKIs: roles beyond cell cycle regulation. Development. 140,
712 3079-3093 (2013).
713 23. D. L. Holiday, V. Speirs. Choosing the right cell line for breast cancer research. Breast Cancer
714 Res. 13, 215 (2011).
715 24. F. L Shaw, H. Harrison, K. Spence, M. P. Ablett, B. M. Simões, G. Farnie, R. B. Clarke. A
716 detailed mammosphere assay protocol for the quantification of breast stem cell activity. J.
717 Mammary Gland Biol. Neoplasia. 17, 111-117 (2012).
718 25. A. Nebbioso, V. Carafa, M. Conte, F. P. Tambaro, C. Abbondanza, J. Martens, M. Nees, R.
719 Benedetti, I. Pallavicini, S. Minucci, G. Garcia-Manero, F. Iovino, G. Lania, C. Ingenito, V.

720 Belsito Petrizzi, H. G. Stunnenberg, L. Altucci. c-MYC Modulation and Acetylation Is a Key
721 HDAC Inhibitor Target in Cancer. Clin. Cancer Res. 23, 2542-2555 (2017).
722 26. A .Yang, S. Qin, B. A. Schulte, S. P. Ethier, K. D. Tew, G. Y. Wang. MYC Inhibition Depletes
723 Cancer Stem-like Cells in Triple-Negative Breast Cancer. Cancer Res. 77, 6641-6650 (2017).
724 27. A. Sulaiman, S. McGarry, X. Han, S. Liu, L. Wang. CSCs in Breast Cancer-One Size Does Not
725 Fit All: Therapeutic Advances in Targeting Heterogeneous Epithelial and Mesenchymal CSCs.
726 Cancers (Basel). 11, E1128 (2019).
727 28. N. Liu, S. Li, N. Wu, K. S. Cho. Acetylation and deacetylation in cancer stem-like cells.
728 Oncotarget. 8, 89315-89325 (2017).
729 29. R. M. Poole. Belinostat: first global approval. Drugs. 74, 1543-1554 (2014).
730 30. E. Seto, M. Yoshida. Erasers of histone acetylation: the histone deacetylase enzymes. Cold Spring
731 Harb. Perspect Biol. 6, a018713 (2014).
732 31. B. C. Valdez, Y. Li, D. Murray, J. E. Brammer, Y. Liu, C. Hosing, Y. Nieto, R. E. Champlin, B.
733 S. Andersson. Differential effects of histone deacetylase inhibitors on cellular drug transporters
734 and their implications for using epigenetic modifiers in combination chemotherapy. Oncotarget.
735 7, 63829-63838 (2016).
736 32. S. Liu, Y. Cong, D. Wang, Y. Sun, L. Deng, Y. Liu, R. Martin-Trevino, L. Shang, S. P.
737 McDermott, M. D. Landis, S. Hong, A. Adams, R. D'Angelo, C. Ginestier, E. Charafe-Jauffret, S.
738 G. Clouthier, D. Birnbaum, S. T. Wong, M. Zhan, J. C. Chang, M. S. Wicha. Breast cancer stem
739 cells transition between epithelial and mesenchymal states reflective of their normal counterparts.
740 Stem Cell Reports. 2, 78-91 (2014).
741 33. G. J. Yoshida. Emerging roles of MYC in stem cell biology and novel tumor therapies. J Exp.
742 Clin. Cancer Res. 37, 173 (2018).
743 34. V. Poli, L. Fagnocchi, A. Fasciani, A. Cherubini, S. Mazzoleni, S. Ferrillo, A. Miluzio, G.
744 Gaudioso, V. Vaira, A. Turdo, M. Gaggianesi, A. Chinnici, E. Lipari, S. Bicciato, S. Bosari, M.

745 Todaro, A. Zippo. MYC-driven epigenetic reprogramming favors the onset of tumorigenesis by
746 inducing a stem cell-like state. Nat. Commun. 9, 1024 (2018).
747 35. A. H. Bild, G. Yao, J. T. Chang, Q. Wang, A. Potti, D. Chasse, M. B. Joshi, D. Harpole, J. M.
748 Lancaster, A. Berchuck, J. A. J.r Olson, J. R. Marks, H. K. Dressman, M. West, J. R. Nevins.
749 Oncogenic pathway signatures in human cancers as a guide to targeted therapies. Nature. 439,
750 353-357 (2006).
751 36. A. Dobin, C. A. Davis, F. Schlesinger, J. Drenkow, C. Zaleski, S. Jha, P. Batut, M. Chaisson, T.
752 R. Gingeras. STAR: ultrafast universal RNA-seq aligner. Bioinformatics 29, 15-21 (2013).
753 37. A. Butler, P. Hoffman, P. Smibert, E. Papalexi, R. Satija. Integrating single-cell transcriptomic
754 data across different conditions, technologies, and species. Nat. Biotechnol. 36, 411-420 (2018).
755 38. X. Chen, J. T. Chang. Planning bioinformatics workflows using an expert system.
756 Bioinformatics. 33, 1210-1215 (2017).
757 39. S. Hänzelmann, R. Castelo, J. Guinney. GSVA: gene set variation analysis for microarray and
758 RNA-seq data. BMC Bioinformatics. 14, 7 (2013).
759
760
761

762 **Acknowledgements**

763 **General:** We thank the anonymous patients used in our study for their generous contributions to research.
764 The AXL inhibitor BGB324 was provided by BerGenBio. Research reported in this publication utilized
765 the High-Throughput Genomics and Bioinformatic Analysis Shared Resource at Huntsman Cancer
766 Institute at the University of Utah.
767
768 **Funding:** This work was supported by the National Cancer Institute of the National Institutes of Health
769 under Award Number P30CA042014. This research was supported by the National Cancer Institute of the

National Institutes of Health under U54 Support Award (1U54CA209978NIH). The content is solely the responsibility of the authors and does not necessarily represent the official views of the NIH. J.T.C. was supported by the Cancer Prevention Research Institute of Texas Core Facility Support Award RP170668. A.H.B and J.T.C were supported by the National Cancer Institute of the National Institutes of Health under award number U54CA209978.

Author Contributions: F.C. and S.W.B. contributed study design and coordination, wrote manuscript, data processing, and analysis. J.L., A. N. and J.C. contributed single cell-RNA sequencing data processing and analysis. P.A.C. contributed single-cell RNA sequencing preparation. M.S. and P.J.M. coordinated sample collection. J.A.M. contributed to data analysis. J.T.C. and M.K. contributed study design. A.H.B. conceived the study, contributed study design and coordination, wrote manuscript, and performed data analysis.

Competing interests: The authors declare no conflict of interest.

Data and materials Availability: Single-cell RNA-seq data for patient#1 and patient#2 from our previous study (Brady et al, 2017) are available on the European Genome-phenome Archive (EGA) under accession EGAS00001002436. Raw and filtered single-cell RNA-seq counts data from patients#5 and patients#6 are available for download at https://doi.org/10.6084/m9.figshare.11374458.v3.

795 **Figures and Tables**

796

797

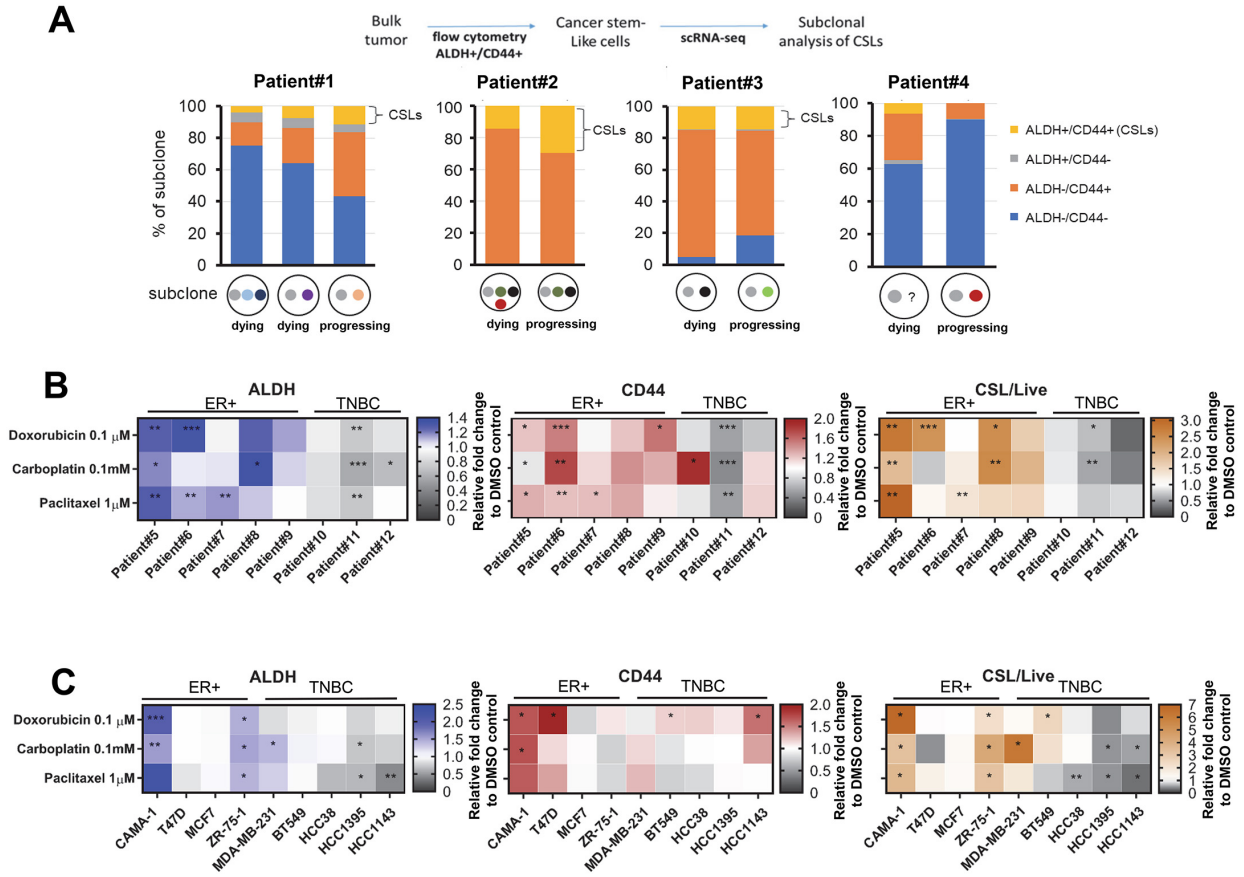

798

799

800

801

802

803 **Fig. 1. Genetic selection and chemotherapy both enrich CSL subclones** . (**A**) The proportion of each
804 subclone with CSL vs. non-CSL populations in four patients. Cells were sorted via FACS using
805 ALDEFLUOR and CD44 staining and DNA was isolated from each population, followed by low-
806 coverage WGS to infer CNV and determine levels of subclonal CNVs. Heat maps for FACS mean values
807 of ALDH, CD44 and CSL cells/Live upon chemotherapy treatment in cultured patient cells (**B**) and breast
808 cancer cell lines (**C**) 3D organoids of patient cells and breast cancer cell lines were incubated with
809 doxorubicin (0.1μM), carboplatin (0.1mM) and paclitaxel (1μM) for 72 hours, followed by
810 ALDEFLUOR/CD44/DAPI staining and FACS to identify the FACS mean values of ALDH and CD44 in
811 live populations and CSL cells/Live. The vehicle controls (DMSO treatment) were set as fold one. All the
812 chemotherapy treatments were expressed as the fold change relative to the control. The mean values of
813 triplicate tests were shown in the heat maps with color indicated as the legends for each treatment.
814 Significance is marked with * for $P<0.05$, ** for $P<0.01$, *** for $P<0.001$.
815

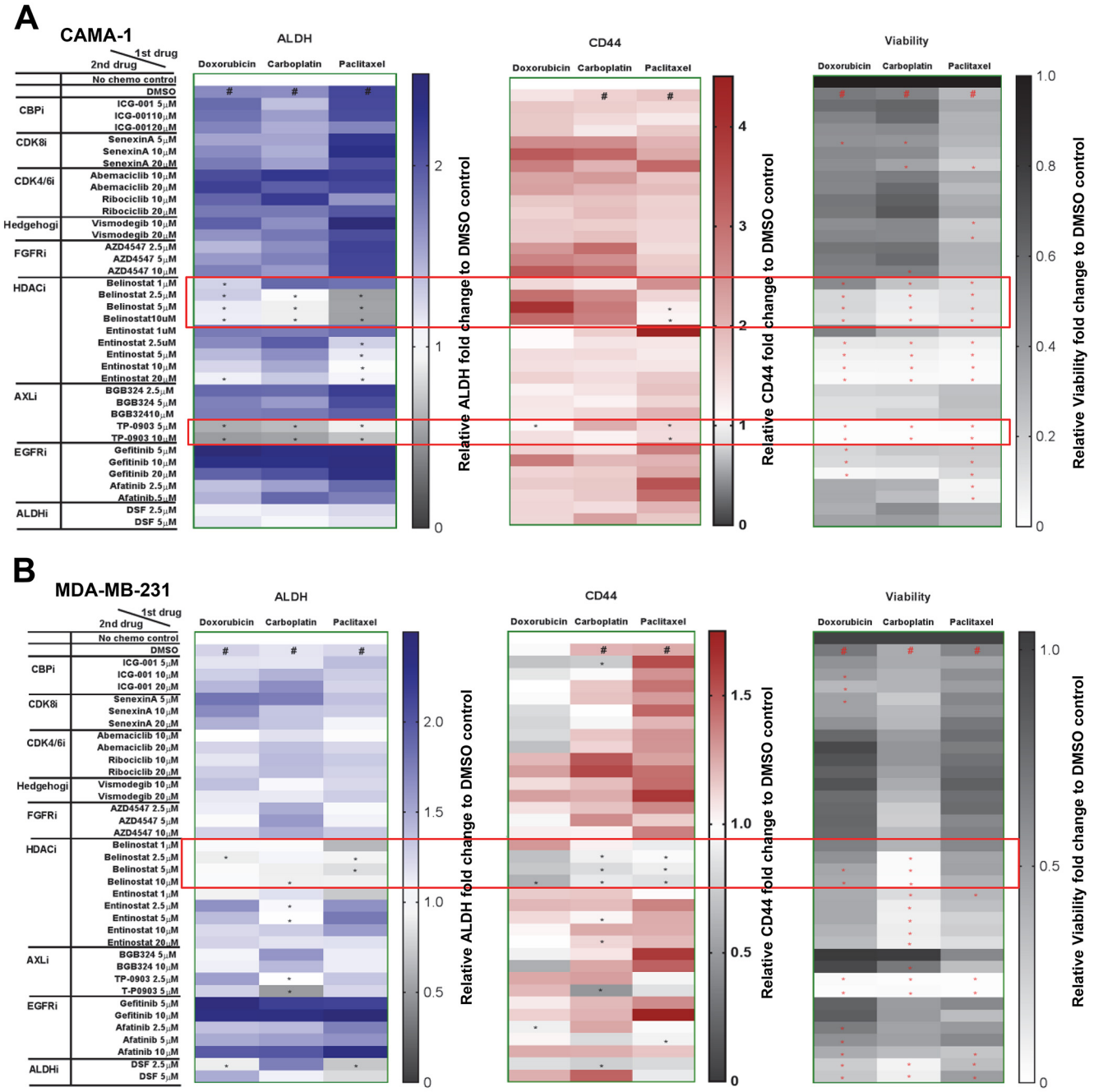
A
CAMA-1
1st drug
2nd drug
ALDH
CD44
Viability
Doxorubicin
Carboplatin
Paclitaxel
No chemo control
DMSO
CBPi
ICG-001 5μM
ICG-00110μM
ICG-00120μM
CDK8i
SenexinA 5μM
SenexinA 10μM
SenexinA 20μM
CDK4/6i
Abemaciclib 10μM
Abemaciclib 20μM
Ribociclib 10μM
Ribociclib 20μM
Hedgehogi
Vismodegib 10μM
Vismodegib 20μM
FGFRi
AZD4547 2.5μM
AZD4547 5μM
AZD4547 10μM
HDACi
Belinostat 1μM
Belinostat 2.5μM
Belinostat 5μM
Belinostat10uM
Entinostat 1uM
Entinostat 2.5uM
Entinostat 5μM
Entinostat 10μM
Entinostat 20μM
AXLi
BGB324 2.5μM
BGB324 5μM
BGB32410μM
TP-0903 5μM
TP-0903 10μM
EGFRi
Gefitinib 5μM
Gefitinib 10μM
Gefitinib 20μM
Afatinib 2.5μM
Afatinib.5μM
ALDHi
DSF 2.5μM
DSF 5μM
Relative ALDH fold change to DMSO control
Relative CD44 fold change to DMSO control
Relative Viability fold change to DMSO control
B
MDA-MB-231
1st drug
2nd drug
ALDH
CD44
Viability
Doxorubicin
Carboplatin
Paclitaxel
No chemo control
DMSO
CBPi
ICG-001 5μM
ICG-001 10μM
ICG-001 20μM
CDK8i
SenexinA 5μM
SenexinA 10μM
SenexinA 20μM
CDK4/6i
Abemaciclib 10μM
Abemaciclib 20μM
Ribociclib 10μM
Ribociclib 20μM
Hedgehogi
Vismodegib 10μM
Vismodegib 20μM
FGFRi
AZD4547 2.5μM
AZD4547 5μM
AZD4547 10μM
HDACi
Belinostat 1μM
Belinostat 2.5μM
Belinostat 5μM
Belinostat 10μM
Entinostat 1μM
Entinostat 2.5μM
Entinostat 5μM
Entinostat 10μM
Entinostat 20μM
AXLi
BGB324 5μM
BGB324 10μM
TP-0903 2.5μM
T-P0903 5μM
EGFRi
Gefitinib 5μM
Gefitinib 10μM
Afatinib 2.5μM
Afatinib 5μM
Afatinib 10μM
ALDHi
DSF 2.5μM
DSF 5μM
Relative ALDH fold change to DMSO control
Relative CD44 fold change to DMSO control
Relative Viability fold change to DMSO control

822 **Fig. 2. Belinostat reduced chemotherapy-promoted CSL state.** Heat maps of FACS mean values for
823 CSL reversal drugs screening with CAMA-1 (**A**) and MDA-MB-231 (**B**) cell lines. Cells were cultured in
824 medium (3D) and treated for 72 hours with doxorubicin (0.1μM for CAMA-1, 0.5μM for MDA-MB-
825 231), carboplatin (50μM for all cell lines), and paclitaxel (1μM for all cell lines), and then treated with
826 potential CSL inhibitors as indicated doses for 72 hours before ALDEFLUOR/CD44 staining. The FACS
827 mean values of ALDH and CD44 in live populations and viability were shown in the heat maps. The
828 vehicle controls (DMSO+DMSO) were set as fold one. All the other chemotherapy plus DMSO/inhibitor
829 combinations were expressed as the fold change relative to the controls. The Chemo plus DMSO served
830 as the positive controls. The mean values of triplicate tests were showed with color indicated as the
831 legends. # is chemo plus DMSO significantly higher ($p<0.05$) than no treatment control, and * is chemo
832 plus inhibitor significantly lower ($p<0.05$) than chemo plus DMSO. The potential inhibitors are
833 highlighted with red blocks as its reversal effect for both ALDH and CD44.
834

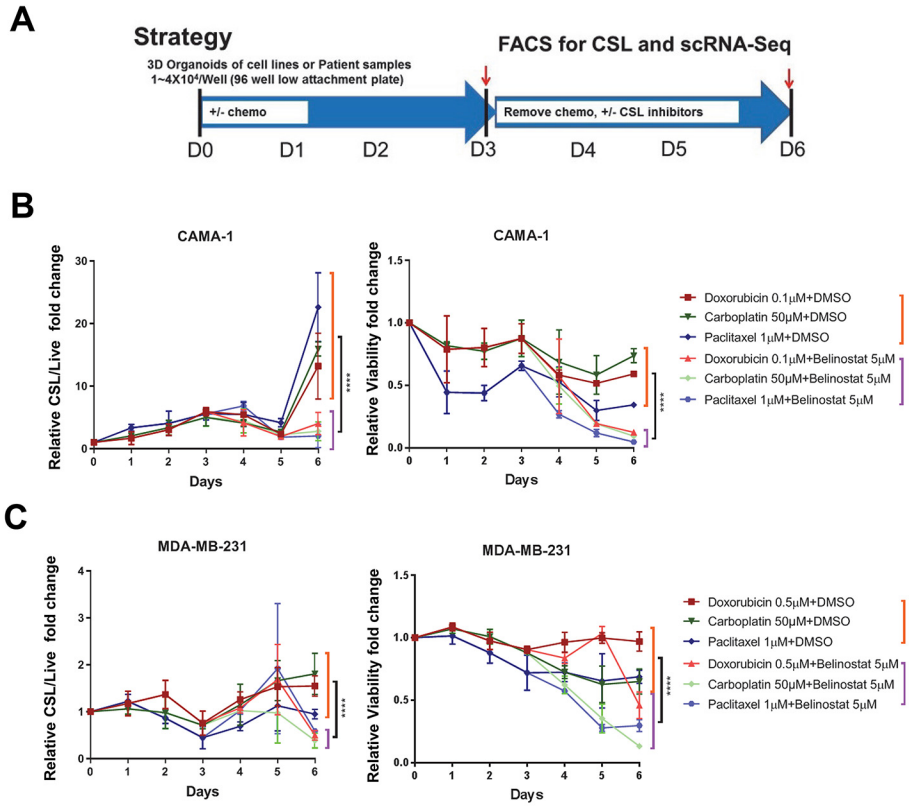
A
Strategy
3D Organoids of cell lines or Patient samples
1~4X10⁴/Well (96 well low attachment plate)
+/- chemo
FACS for CSL and scRNA-Seq
Remove chemo, +/- CSL inhibitors
D0
D1
D2
D3
D4
D5
D6
B
CAMA-1
Relative CSL/Live fold change
Days
CAMA-1
Relative Viability fold change
Days
Doxorubicin 0.1μM+DMSO
Carboplatin 50μM+DMSO
Paclitaxel 1μM+DMSO
Doxorubicin 0.1μM+Belinostat 5μM
Carboplatin 50μM+Belinostat 5μM
Paclitaxel 1μM+Belinostat 5μM
C
MDA-MB-231
Relative CSL/Live fold change
Days
MDA-MB-231
Relative Viability fold change
Days
Doxorubicin 0.5μM+DMSO
Carboplatin 50μM+DMSO
Paclitaxel 1μM+DMSO
Doxorubicin 0.5μM+Belinostat 5μM
Carboplatin 50μM+Belinostat 5μM
Paclitaxel 1μM+Belinostat 5μM

835

836

837

838 **Fig. 3. Belinostat inhibited chemotherapy-promoted CSL state in a time-dependent manner.** (**A**)
839 Cell culture strategy for CSL reversal drug screening with cancer breast cell lines after chemo promotion.
840 The CSL cells/live (ALDH+, CD44+ cells versus live cells) and viability are shown in (**B**) for CAMA-1
841 and (**C**) for MDA-MB-231 with curves. CAMA-1 cells and MDA-MB-231 cells were cultured in medium
842 (3D) and treated for 72 hours with doxorubicin (0.1μM for CAMA-1, 0.5μM for MDA-MB-231),
843 carboplatin (50μM), and paclitaxel (1μM), and then replaced with medium containing belinostat (5μM)
844 for 72 hours incubation. Samples were collected every day from Day 0 to Day 6, and subjected to
845 ALDEFLUOR/CD44/DAPI staining followed by FACS. In each day, DMSO treatment served as control
846 and was set as fold one. All the other treatments were expressed as the fold values relative to the controls.
847 Each spot represents the mean value of triplicate tests. The differences between chemo plus DMSO (9
848 replicates from three chemo plus DSMO) and chemo plus belinostat (9 replicates from three chemo plus
849 belinostat) at Day 6 were evaluated by student's T tests. Significance is marked with * for P<0.05, ** for
850 P<0.01, *** for P<0.001, *** for P<0.0001, **** for P<0.0001.
851

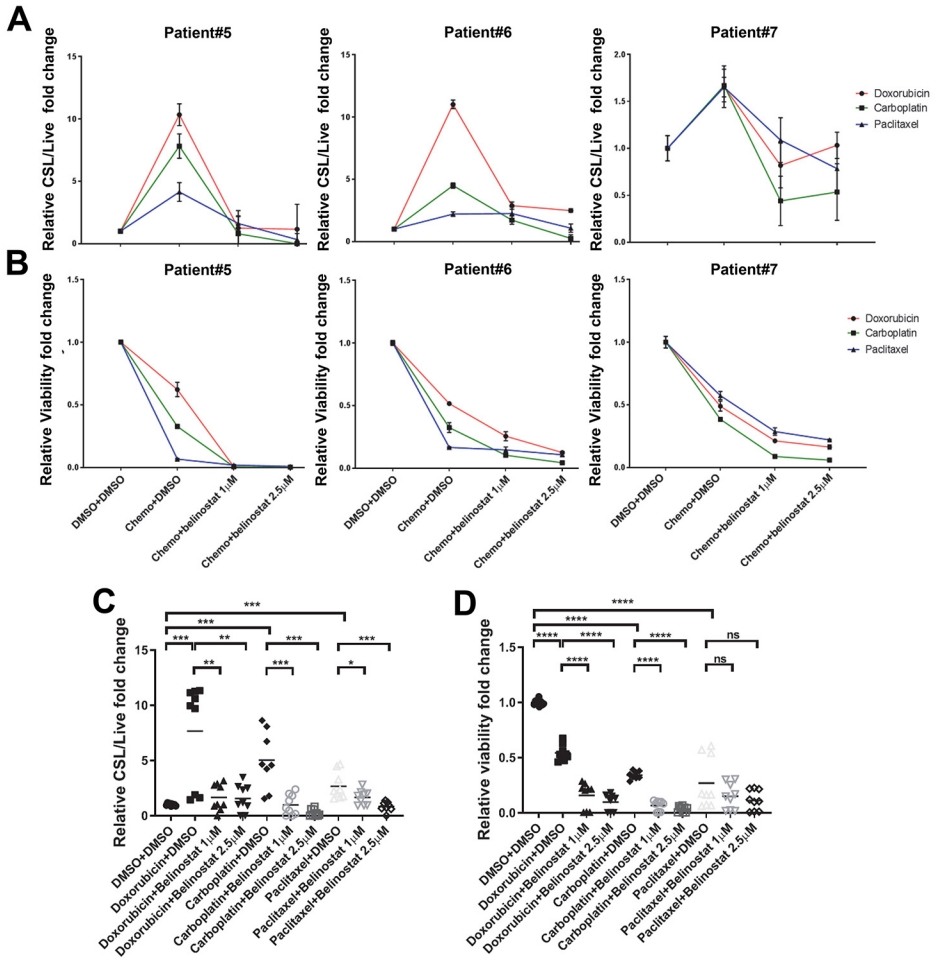
A
Patient#5
Patient#6
Patient#7
Relative CSL/Live fold change
Doxorubicin
Carboplatin
Paclitaxel
B
Relative Viability fold change
DMSO+DMSO
Chemo+DMSO
Chemo+belinostat 1μM
Chemo+belinostat 2.5μM
C
Relative CSL/Live fold change
D
Relative viability fold change
ns

852

853

854 **Fig. 4. Belinostat reversed chemotherapy-induced CSL cells in ER+ patient samples.** (**A**) The CSL
855 cells/live (ALDH+, CD44+ cells versus live cells) and (**B**) viability were expressed with curves for
856 Patient#5, #6, and #7. Patient cells were cultured in Renaissance medium (3D) and treated with
857 chemotherapy (doxorubicin 0.1 μM, carboplatin 0.1mM, paclitaxel 1μM) for 72 hours, and then treated
858 with DMSO/belinostat (1μM or 2.5 μM) for another 72 hours, followed by ALDEFLUOR/CD44/DAPI
859 staining and FACS analysis. DMSO treatment only (DMSO+DMSO) served as controls and was set as
860 fold one. All the other treatments were expressed as the fold values relative to the controls. Each spot in
861 (**A**) and (**B**) represents the mean values of triplicate tests. Column graphs with individual values were
862 generated by combining 9 replicates from three patients for each treatment to evaluate the changes in CSL
863 cells/live (**D**) and viability (**E**). The statistical analysis was performed with student's t-tests between the
864 indicated groups with triplicate tests. Significance is marked with * for $P<0.05$, ** for $P<0.01$, *** for
865 $P<0.001$, **** for $P<0.0001$.
866
867
868
869
870
871

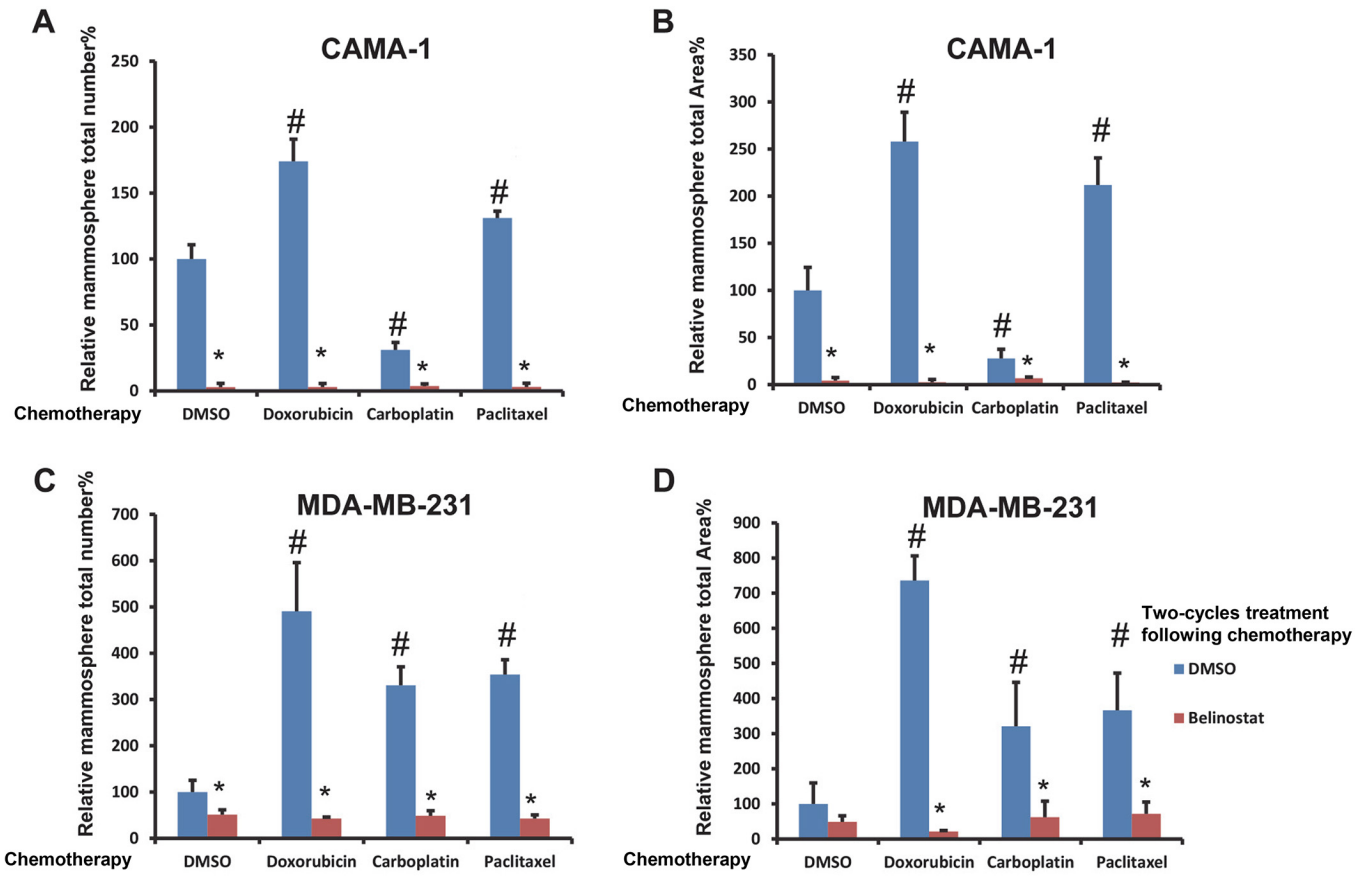

872
873

874

875

876

877

878

879 **Fig. 5. Belinostat inhibited mammosphere formation of chemotherapy-treated breast cancer cell**
880 **lines.** CAMA-1 and MDA-MB-231 cells from spheroids with 3 days chemo treatment (DMSO,
881 doxorubicin 0.1μM for CAMA-1, 0.5μM for MDA-MB-231, carboplatin 50μM, and paclitaxel 1μM)
882 were collected, dissociated, and cultured for two 14 days periods with mammosphere assay medium
883 containing DMSO/belinostat (5μM) as described in the Methods. Mammosphere total numbers and total
884 area of CAMA-1 are shown in (**A**) and (**B**). Mammosphere total numbers and total area of MDA-MB-231
885 are shown in (**C**) and (**D**). The treatments with DMSO only serve as the control in each figure and set as
886 fold one. All the other treatments are expressed relative to the controls in the figures. The statistical
887 analysis was performed with student's t-tests between the indicated groups with triplicate tests. # is
888 $p<0.05$ relative to DMSO plus DMSO only, * is $p<0.05$ relative to chemo plus DMSO.
889
890
891
892
893
894
895
896
897
898
899
900
901
902
903

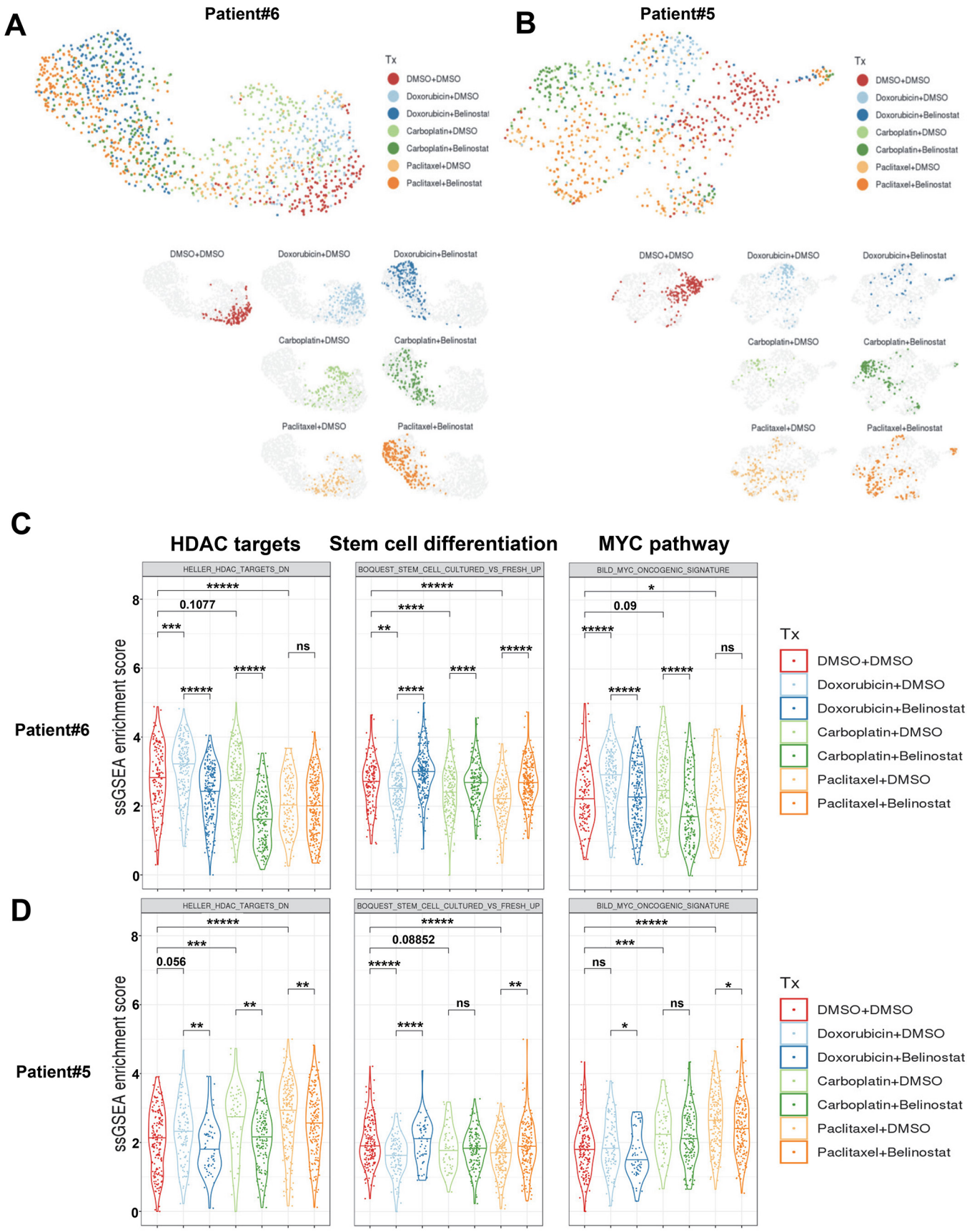
A
Patient#6
B
Patient#5
Tx
DMSO+DMSO
Doxorubicin+DMSO
Doxorubicin+Belinostat
Carboplatin+DMSO
Carboplatin+Belinostat
Paclitaxel+DMSO
Paclitaxel+Belinostat
C
HDAC targets
Stem cell differentiation
MYC pathway
HELLER_HDAC_TARGETS_DN
BOQUEST_STEM_CELL_CULTURED_VS_FRESH_UP
BILD_MYC_ONCOGENIC_SIGNATURE
Patient#6
ssGSEA enrichment score
0.1077
0.09
D
Patient#5
0.056
0.08852

904

905 **Fig. 6. Chemotherapy and belinostat reprogrammed transcriptome of patient cells.** Unbiased
906 UMAPs for ER+ patient sample Patient#6 (**A**) and Patient#5 (**B**) under treatment (Tx). Patient cells were
907 cultured in Renaissance medium (3D) and treated with chemotherapy (doxorubicin 0.1 μM, carboplatin
908 0.1mM, paclitaxel 1μM) for 72 hours, and then treaded with DMSO/belinostat (1μM) for 72 hours. The
909 cells were collected, purified with Dead Cell Removal Kit, and subjected to ICELL8® Single-Cell
910 System as described in Methods. For each patient, the UMAPs for all treatments were shown in the top,
911 and the UMAPs for each individual treatment were shown in the bottom with different colors indicated as
912 the legends. Violin plots with GSEA pathways enrichment scores related to HDAC targets, stem cell
913 differentiation and MYC pathway were presented in (C) for Patient#6 and (D) for Patient#5. The
914 statistical analysis was performed with student's t-test between the indicated groups, and significance is
915 marked with * for P<0.05, ** for P<0.01, *** for P<0.001, **** for P<0.0001.
916
917 \
918